

REACTOR NEUTRINO PHYSICS - AN UPDATE *

FELIX BOEHM

*Physics Department, California Institute of Technology,
Pasadena, CA 91125, USA*

E-mail: boehm@caltech.edu

ABSTRACT

We review the status and the results of reactor neutrino experiments. Long baseline oscillation experiments at Palo Verde and Chooz have provided limits for the oscillation parameters while the recently proposed Kamland experiment at a baseline of more than 100km is now in the planning stage. We also describe the status of neutrino magnetic moment experiments at reactors.

1. The Reactor Neutrino Spectrum

Nuclear reactors provide high flux low energy neutrinos and are thus well suited for exploring $\bar{\nu}_e$ disappearance for small values of the mass parameter Δm^2 . As the neutrino energy E_ν enters as the ratio L/E_ν , L being the distance between reactor and detector, a reactor experiment with E_ν around 5 MeV at $L = 1$ km has the same sensitivity to Δm^2 as an accelerator experiment with $E_\nu = 5$ GeV at 1,000 km.

The reactor neutrino flux and the neutrino-proton cross sections are depicted together with their product in Fig. 1¹.

2. Oscillation Experiments

The results from atmospheric neutrino experiments, such as those from Kamiokande² have triggered reactor neutrino studies in the parameter region Δm^2 between 10^{-2} and 10^{-3} eV^2 . Two experiments, both at L around 1 km, have been conducted recently, one at the French reactor at Chooz³ and the other at the Palo Verde⁴ site in Arizona, USA. Both experiments now have results and we shall describe them below. Another experiment, the Kamland⁵ experiment, at a much larger distance, is still in the proposal stage. To illustrate the effect from oscillations on the positron spectrum, we show in Fig. 2 the expected spectrum for Chooz or Palo Verde for the case of no oscillations as well as for the set of oscillation parameters favored by the Kamiokande. Clearly, the effects on the spectrum are quite pronounced.

The Chooz and the Palo Verde experiments are based on the inverse neutron decay reaction, $\bar{\nu}_e + p = e^+ + n$, and rely on a measurement of both, the e^+ and the n as a correlated signature. Both experiments make use of Gd loaded liquid scintillator. Gd loading reduces the capture time owing to its large thermal neutron capture cross section, and also gives rise to a high energy gamma cascade of up

*Invited talk at the 8th Int. Workshop on "Neutrino Telescopes", Venice, February 1999.

to 8 MeV. Both features are valuable, the short capture time helps reduce random coincidences and the large gamma ray energy allows reduction of backgrounds as the energy threshold can be set above that of radioactive decay products. In both experiments the amount of Gd dissolved in the scintillator is about 0.1% by weight. At a distance of ca 1 km from the reactor the detector response is about 5 events per day per ton of scintillator. The Chooz experiment takes advantage of an existing deep tunnel reducing the cosmic ray muon background substantially, while the Palo Verde experiment being in a shallow underground laboratory has to cope with a larger muon rate. Because of this difference in shielding, the two detectors had to be designed differently. While the Chooz detector consists of a homogeneous central volume of Gd scintillator, the Palo Verde detector is made from finely segmented detector cells.

3. The Palo Verde Experiment

The Palo Verde experiment, a collaboration⁴ between Caltech, Stanford University, University of Alabama, and Arizona State University, is installed near the Palo Verde nuclear power plant (3 reactors, 11 GW thermal power) in the desert to the west of Phoenix, Arizona. The detector is installed in an underground cave with 32 mwe overhead at a distance of $L = 890$ m from reactors 1 and 3, and 750 m from reactor 2. Each reactor is shut down for refueling for a period of ca 40 days every year which allows us to obtain background data.

The detector, shown schematically in Fig. 3, has a fiducial volume of 12 tons. Its liquid scintillator, whose composition is 60% mineral oil, 36% pseudocumene, 4% alcohol, and 0.1% Gd, was developed in collaboration with Bicorn⁶. It has an effective light attenuation length of 10m for 440nm light. There are 66 cells, each 9m long, of which 7.4m are active and 0.8m on each end serve as an oil buffer. There is a 5 inch low radioactivity *ElectronTubes* photomultiplier attached to each end, allowing both, the anode and the last dinode to be read out. A blue LED installed at 0.9m from each PM, as well as optical fibers, allow each individual cell to be monitored. A passive water shield, 1m thick, surrounds the block of active cells to help shield against radioactivity as well as muon induced neutrons. An active veto counter consisting of 32 12m long MACRO cells is placed on all 4 long sides while a removable end-veto counter protects the ends of the cell matrix.

A diagram of the detector response showing the $\bar{\nu}_e$ reaction and the gamma rays from Gd capture is given in Fig. 4.

A neutrino signal consists of a fast (30ns) $e^+\gamma\gamma$ trigger within a block of 3 x 5 cells, with the first hit having $E \geq 500keV$, and the second hit $E \geq 30keV$. This second hit includes the Compton response from the 511 keV annihilation gammas. This fast triple coincidence is followed by a slow (200 μs) signal due to the 8 MeV

gamma cascade following neutron capture in Gd within a 5 x 7 scintillator cell matrix.

3.1. Calibrations

Energy calibrations were carried out with the help of small sources that were introduced through a set of Teflon tubes installed alongside a group of detector cells. The sources were ^{228}Th (2.6 MeV γ) depicted in Fig. 5, ^{65}Zn , ^{137}Cs , and ^{57}Co (0.12 MeV). Response from these sources at various positions allowed us to determine and monitor the attenuation length of the scintillator. We found only a negligible decline over the period measured. Fig. 6 shows the light yield along the scintillator cell.

The PMT linearity was obtained with the help of a fiber optics flasher. Single photo-electron peaks were monitored with a blue LED.

To obtain the positron efficiency of the detector, we used the positron emitter ^{22}Na . A calibrated ^{68}Ge source⁷ dissolved in a special cell will be implemented later in the experiment. The neutron efficiency was obtained with the help of a calibrated AmBe source. This source had a strength of 150 n/s and was used in a tagged mode, i.e. in coincidence with the 4.4MeV gamma from $^{12}\text{C}^*$. The average efficiency (over the detector) was also calculated with the help of a Monte Carlo simulation. For our cuts, the resulting efficiency was found to be 0.159. Combined with a data acquisition efficiency of 0.82 and a veto-live efficiency at our veto rate of 2 kHz, we determined the total efficiency for observing a neutrino to be 0.082.

We calculated the number of neutrino interactions in the detector for the case of no-oscillations from the neutrino flux from the 3 reactors, the cross section and the number of protons in the detector, and found (for a given moment in the fuel cycle) an interaction rate of 201 ± 2 per day.

3.2. Results from the first 72 days of data

We now present an early data set consisting of 39 days (November and December 1998) of data with 3-reactors-on and 33 days (October 1998) of data with 2-reactors-on (reactors at 890m and 750m) corresponding to a ν flux of 100% and 71%, respectively. The event rates were found to be 39.1 ± 1.0 (st) per day and 32.6 ± 1.0 per day, respectively, with a difference of 6.4 ± 1.4 (st) attributed to the 890m reactor. The signal-to-background ratio was found to be 1.2. Corrected for efficiency, the number of neutrino interactions from the 890m reactor was found to be 77 ± 17 (st) ± 11 (sys) per day. This is to be compared with the calculated number for the 890m reactor of 59 ± 2 per day. The correlated positron spectra (fourfold coincidences) are shown in Fig. 7 and the time structure for these events from the data and from Monte Carlo is given in Fig. 8 from where it can be seen that the effective neutron capture time in our detector is $35\mu\text{s}$.

In Fig. 9 we show the exclusion plot obtained from our 72 day data run, together

with the parameter range allowed from the Kamiokande atmospheric results. Our results rule out $\nu_\mu \leftrightarrow \nu_e$ oscillations at the 90% confidence level, in agreement with the results from the Chooz experiment to be discussed below.

3.3. The neutron angular distribution

The segmentation of our detector allows us to study the neutrino-neutron angular correlation and to use it for independent background determinations. From kinematics we find that the neutron moves preferentially in the direction of the incoming neutrino, with an angular distribution

$$\cos(\theta_{\nu,n})_{max} = [2\Delta/E_\nu - (\Delta^2 - m^2)/E_\nu^2]^{1/2}, \quad (1)$$

where $\Delta = M_n - M_p$.

From Monte Carlo simulation it is found that the neutron scattering largely preserves the angular distribution, resulting in a shift of the mean coordinate of the neutron capture center $\langle x \rangle = 1.7 \text{ cm}^8$. The angular spread after scattering is very pronounced as can be seen in Fig. 10. It should be noted that this effect was first studied by Zacek⁹ in connection with the segmented Goesgen detector where the forward/backward ratio was found to be as large as a factor of 2.

Results from our first run give an asymmetry expressed as events in the half plane away from the reactor (forward) minus events in the half plane toward the reactor (backward) of 109 ± 44 , in agreement with a Monte Carlo simulation.

3.4. Plans for the future of the Palo Verde experiment

We plan to continue data runs through 1999, a period which includes two refueling cycles, giving us a tenfold larger statistical accuracy and correspondingly larger sensitivity to the mixing angle. We shall continue to make use of the forward-backward asymmetry and we shall also implement a ^{68}Ge run to determine the detector efficiency with higher accuracy.

4. The Chooz Experiment

An experiment with similar aim, however with a somewhat different detector was carried out at Chooz by a French-Italian-Russian-US collaboration³ This experiment and its results have been published, and we will review it here with just a few highlights.

The Chooz detector is comprised of three regions, a central region containing 5 tons of Gd loaded liquid scintillator and surrounded by an acrylic vessel, a containment region with 17 tons of ordinary liquid scintillator, and an outer veto region with 90 tons of scintillator.

Fig. 11 shows schematically the arrangement of the Chooz detector.

The inner two regions are viewed by a set of photomultipliers. An independent set of PM detects the light from the veto region. While the positron response is obtained from a signal in the inner region, the neutron response comprises signals from the inner region as well as from the containment region, resulting in a well contained and well resolved Gd capture sum peak at 8 MeV. As mentioned earlier, the Chooz detector is installed in a tunnel, thus reducing the correlated background to less than 10% of the signal.

The published data was obtained at various power levels of one of the two Chooz reactors. A total of 1320 neutrino events was accumulated in 2718 live hours. Normalized to the full power of the two reactors (8.5 GW th) the event rate corresponds to 25.5 ± 1.0 per day where the error includes contributions from the reaction cross section, the reactor power, and the number of protons in the target. The ratio of measured-to-expected neutrino signal is 0.98 ± 0.04 (st) ± 0.04 (sys). The reactor-off rate was 1.2 ± 0.3 per day. The total efficiency of the detector was found to be 0.71 ± 0.02 .

The positron energy spectrum for reactor-on and reactor-off is shown in Fig. 12, together with a plot of the ratio of measured-to-calculated spectrum.

Fig. 13 shows the Chooz exclusion plot. Clearly, the Kamiokande region is excluded with high confidence level, implying the absence of $\nu_\mu \leftrightarrow \nu_e$ oscillations. The mixing angle limit for large Δm^2 from this analysis is $\sin^2 2\theta < 0.18$ at 90% CL. While an analysis based on the widely accepted method by Feldman and Cousins¹⁰ gives $\sin^2 2\theta < 0.22$ (90%). The 90% limit for Δm^2 for maximum mixing from this experiment is $0.9 \times 10^{-3} eV^2$.

Recently, the Chooz collaboration has compared the spectrum from reactor 2 which is at $L = 998\text{m}$ to that of reactor 1 at $L = 1115\text{m}$. The relative spectra from the two reactors at different distances provide information on oscillations which is independent of the absolute yields. Their analysis leads to an exclusion plot consistent with, however less stringent than that of Fig. 13. The relative positron yield is $Y(1115\text{m}) / Y(998\text{m}) = 0.96 \pm 0.06$ (st) ± 0.015 (sys).

The Chooz collaboration has completed data taking and is now finalizing the data analysis. Their analysis will also include a discussion of the neutron angular distribution as mentioned in the section above on Palo Verde.

5. The Kamland Experiment

The Kamland⁵ experiment described by A. Suzuki in the following lecture will be the ultimate long baseline reactor experiment, destined to explore $\bar{\nu}_e$ disappearance at very small Δm^2 . It will be sensitive to exploring the large mixing angle solar MSW solution. The experiment will also address the small mixing angle solar MSW at low neutrino energy, as well as, by invoking seasonal variations, the "just so" solution.

The neutrinos originate from 16 nuclear power reactors at distances between 100 km and 300 km from the Kamland detector. The detector will be a 1 kT liquid scintillator to be installed in the former Kamiokande cavity. With an expected event rate of 1075/y the sensitivity to Δm^2 will be $4 \times 10^{-6} eV^2$.

6. Neutrino Magnetic Moment

If neutrinos have mass, they may have a magnetic moment. An experimental effort to look for a neutrino magnetic moment, therefore, is of great interest. Some indications for a magnetic moment have come from the apparent correlation of the signal in the ^{37}Cl experiment with solar activity, suggesting a value of $10^{-11} - 10^{-10} \mu_{Bohr}$. In addition, considerations of a possible resonant spin flavor precession (RSFP), and also of neutrino interactions in supernovae have been mentioned.

The neutrino magnetic moment contributes to the $\nu_e e$ scattering¹¹ as shown in Fig. 14. This contribution is most pronounced at low electron-recoil energy. At about 300 keV the magnetic moment scattering is roughly equal to the weak scattering.

Previous results by Reines et al.¹² from scattering reactor neutrinos on electrons in a 16 kg plastic scintillator have given $\mu_\nu = 2 - 4 \times 10^{-10} \mu_B$. More recently, Gurevitch et al.¹³, using a 103kg C_6F_6 target have found $\mu_\nu < 2.4 \times 10^{-10} \mu_B$, and Derbin et al.¹⁴ with a 75kg Si target have found $\mu_\nu < 1.8 \times 10^{-10} \mu_B$.

An effort to obtain a value or stringent limit of μ_ν is now underway by the MUNU experiment, a Grenoble-Munster-Neuchatel-Padova-Zurich collaboration¹⁵ which has built a 1000 liter CF_4 TPC at 5atm (18.5kg), surrounded by an anti-Compton shield. This detector is now installed at the Bugey reactor in France. The expected event rate in the interval of 0.5 to 1 MeV recoil energy is 5.1 per day, at an expected background of 4.5 per day. Implementing the angular correlation of the scattered electrons with respect to the incoming reactor neutrinos is expected to enhance the signal-to-noise significantly. A schematic view of the MUNU TPC is shown in Fig. 15.

7. Conclusion

Reactor neutrinos with their low energies are well suited to explore small Δm^2 for the $\bar{\nu}_e$ disappearance channel. From the results of the Chooz and Palo Verde experiments it can be concluded that the atmospheric ν_μ deficiency cannot be attributed to $\bar{\nu}_\mu \leftrightarrow \bar{\nu}_e$ oscillations. The Chooz experiment has ruled out this channel with large confidence level, and the first data set from Palo Verde excludes it at 90% CL. To improve on the mixing angle sensitivity in these experiments so as to shed light on a possible 3-flavor solution will be a challenging task. The Kamland experiment at very large baseline is now on the drawing board. Searches for a neutrino magnetic moment from the MUNU experiment are in progress.

1. P. Vogel, private communication.
2. Y. Fukuda et al., *Phys.Lett.B* **335** (1994) 237.
3. M. Apollonio et al., *Phys.Lett.B* **420** (1998) 397; Bemporad, "Neutrino 98", *Int. Conf. Neutrino Physics and Astrophysics*, Takayama (1998).
4. *The Palo Verde Collaboration*, F. Boehm, B. Cook, J. Hansen, H. Henrikson, K.B. Lee, D. Michael, V.M. Novikov, A. Piepke, and P. Vogel (Caltech); G. Gratta, L. Miller, D. Tracy, and F.Y. Wang (Stanford University); J. Busenitz, J. Kornis, A. Vital, and J. Wolf (University of Alabama); D. Lawrence and B. Ritchie (Arizona State University); <http://citnp.caltech.edu/PV/Palo-Verde.html>.
5. A. Suzuki, this Conference.
6. A. Piepke et al., *Nucl.Instr.Meth.A*, submitted for publication (1999).
7. A. Piepke and B. Cook, *Nucl.Instr.Meth.A* **385** (1996) 85.
8. P. Vogel and J. F. Beacom, preprint *hep-ph/9903554*, *Phys.Rev.D*, to be published; K.B. Lee, private communication.
9. G. Zacek, Thesis, Technical University of Munich (1984).
10. G.J. Feldman and R.D. Cousins, *Phys.Rev.D* **57** (1998) 3873.
11. P. Vogel and J. Engel, *Phys.Rev.D* **39** (1989) 3378.
12. F. Reines et al., *Phys.Rev.Lett.* **37** (1976) 315.
13. I.I. Gurevitch et al., *JETP Lett.* **49** (1989) 740.
14. A.I. Derbin et al., *JETP Lett.* **57** (1993) 768.
15. C. Amsler et al., *Nucl.Instr.Meth.A* **396** (1997) 115.

8. Figure Captions

Fig. 1. Energy spectrum, cross section and yield of neutrinos from a reactor.

Fig. 2. Expected positron spectra for the Chooz or Palo Verde experiment for "no oscillations" and for oscillations given by the Kamiokande parameters.

Fig. 3. Schematic view of the Palo Verde detector.

Fig. 4. Illustration of the neutrino reaction in the matrix of Gd loaded scintillator.

Fig. 5. Energy spectrum from a ^{228}Th source ($E_\gamma = 2.6$ MeV).

Fig. 6. Light yield along scintillator cell. The attenuation length of the Gd scintillator is 10m.

Fig. 7. Correlated positron spectrum from a 3-reactor run (100% ν flux) and a 2-reactor run (71% flux).

Fig. 8. Decay time of the fourfold coincidence gives the neutron capture time in our Gd-scintillator.

Fig. 9. Region in the parameter space excluded at 90% CL for our 72 day run. Most of the Kamiokande allowed region can be excluded from this data.

Fig. 10. Angular distribution of scattered (moderated) neutrons with regards to the neutrino direction.

Fig. 11. Schematic arrangement of the Chooz detector.

Fig. 12. Positron energy spectra from the Chooz experiment.

Fig. 13. Exclusion plot from the Chooz experiment.

Fig. 14.

Contribution of the neutrino magnetic moment to the $\bar{\nu}_e e \rightarrow \bar{\nu}_e e$ scattering, averaged over the reactor $\bar{\nu}_e$ spectrum. The purely weak cross section is also shown. (From Vogel and Engel¹¹)

Fig. 15. Layout of the MUNU detector for the measurement of the neutrino magnetic moment.

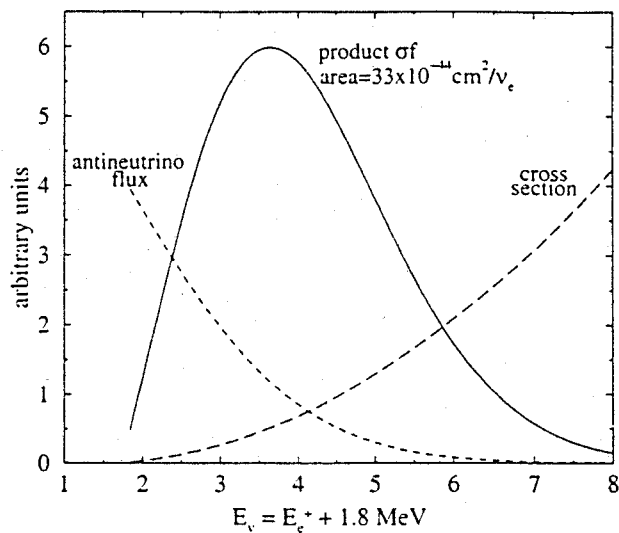


Fig. 1. Energy spectrum, cross section and yield of neutrinos from a reactor.

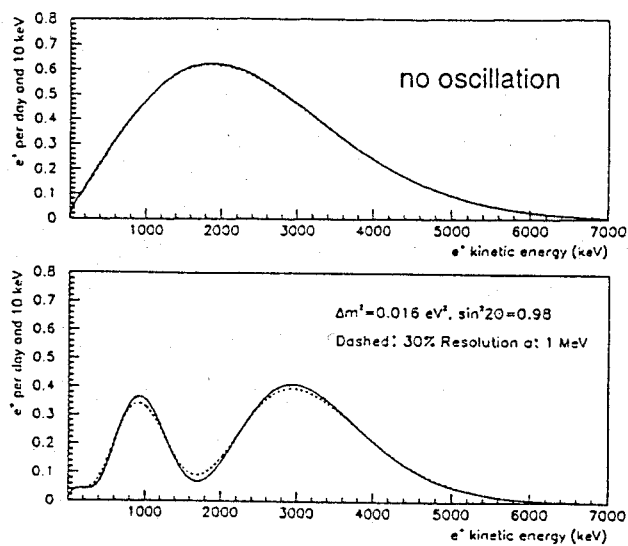


Fig. 2. Expected positron spectra for the Chooz or Palo Verde experiment for "no oscillations" and for oscillations given by the Kamiokande parameters.

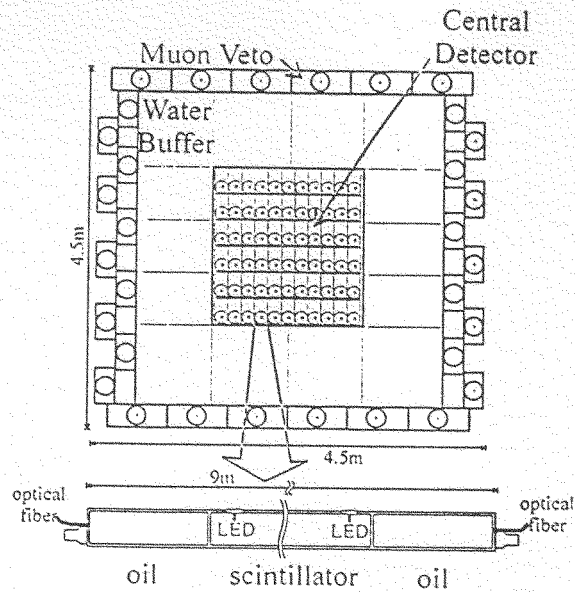


Fig. 3. Schematic view of the Palo Verde detector.

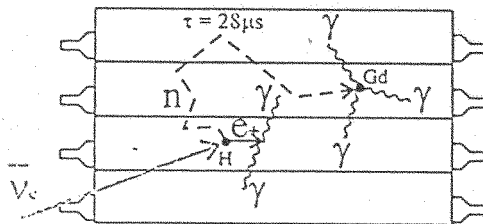


Fig. 4. Illustration of the neutrino reaction in the matrix of Gd loaded scintillator.

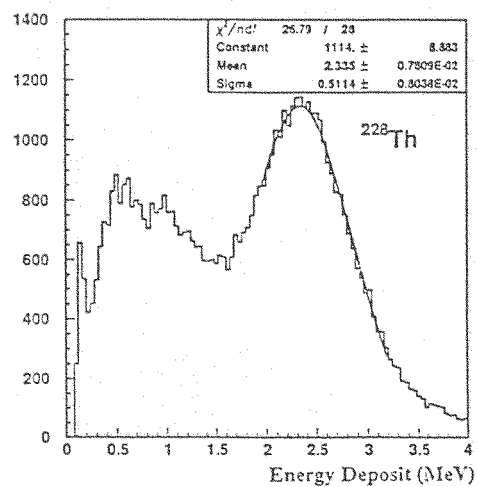


Fig. 5. Energy spectrum from a ^{228}Th source ($E_\gamma = 2.6 \text{ MeV}$).

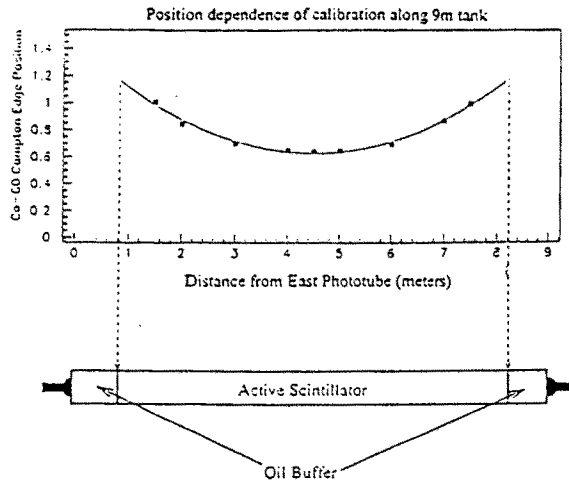


Fig. 6. Light yield along scintillator cell. The attenuation length of the Gd scintillator is 10

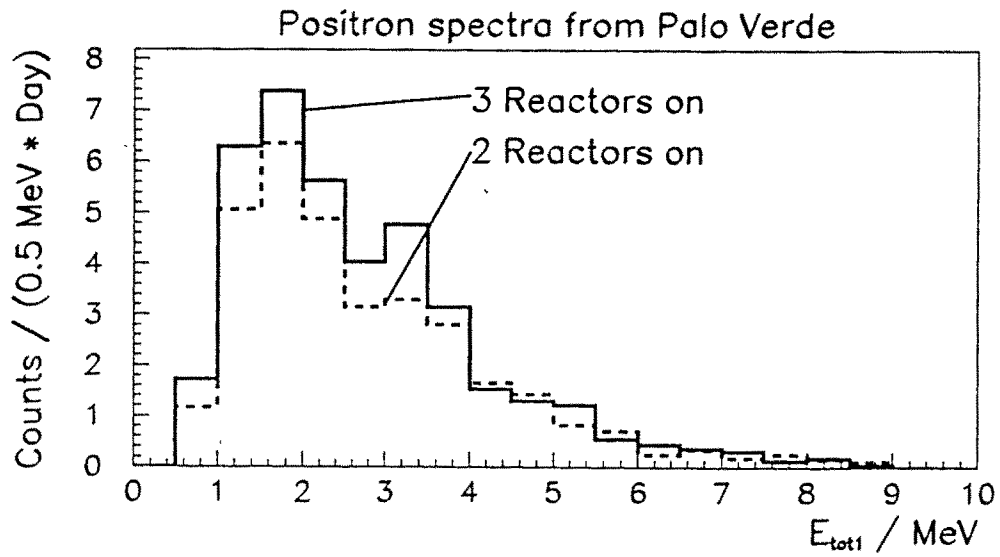
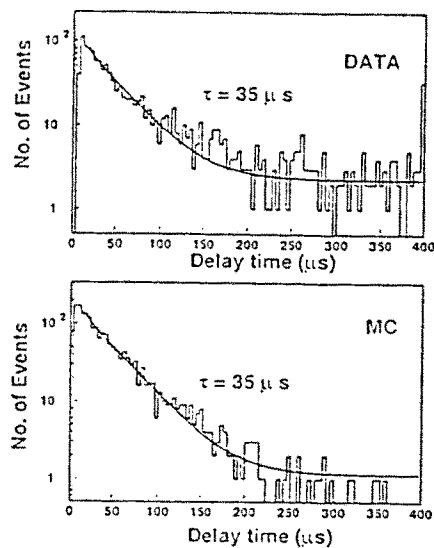


Fig. 7. Correlated positron spectrum from a 3-reactor run (100% ν flux) and a 2-reactor run (71% flux).



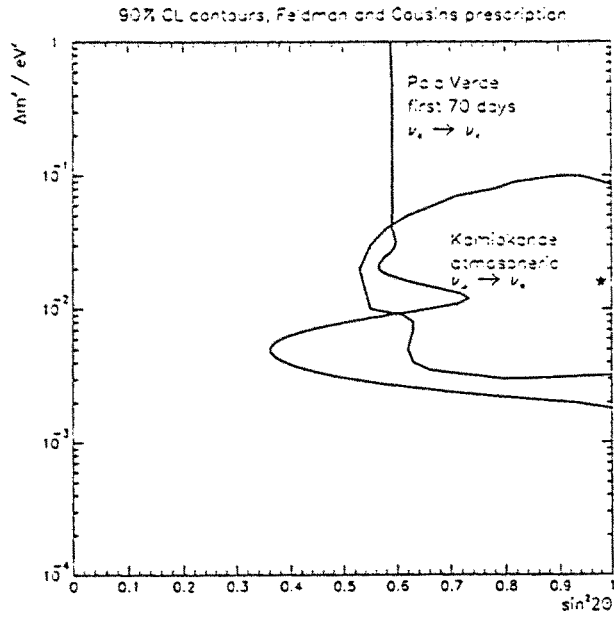


Fig. 9. Region in the parameter space excluded at 90% CL for our 72 day run. Most of the Kamiokande allowed region can be excluded from this data.

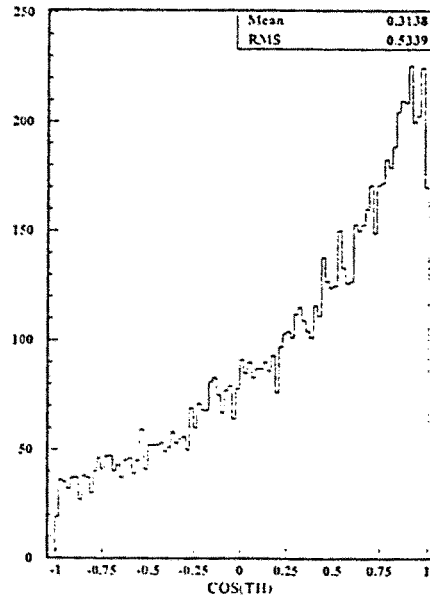


Fig. 10. Angular distribution of scattered (moderated) neutrons with regards to the neutrino direction.

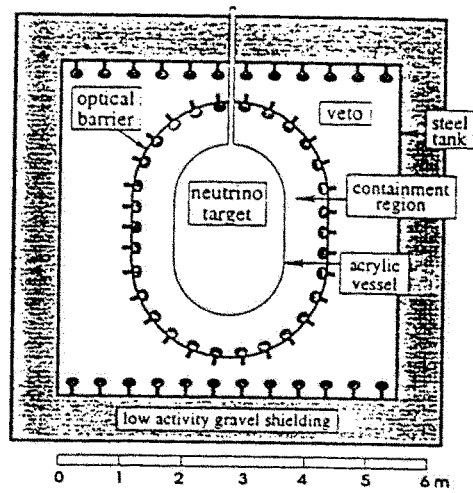


Fig. 11. Schematic arrangement of the Chooz detector

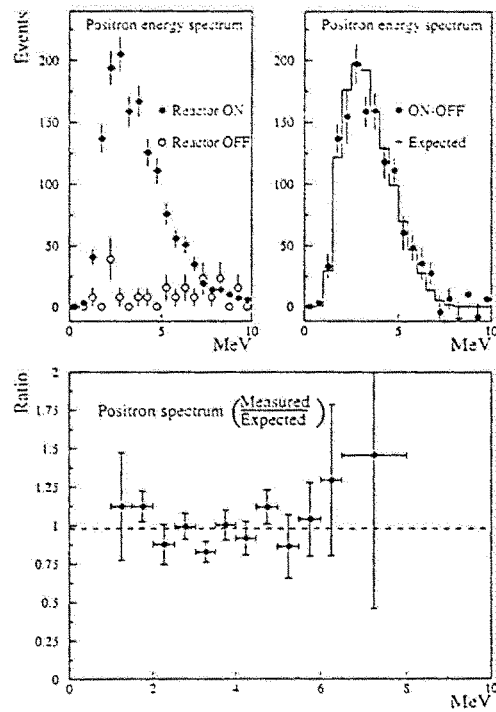


Fig. 12. Positron energy spectra from the Chooz experiment.

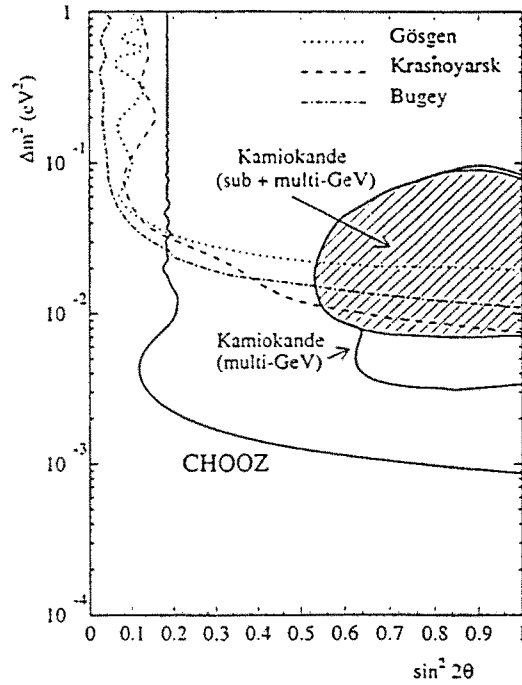


Fig. 13. Exclusion plot from the Chooz experiment.

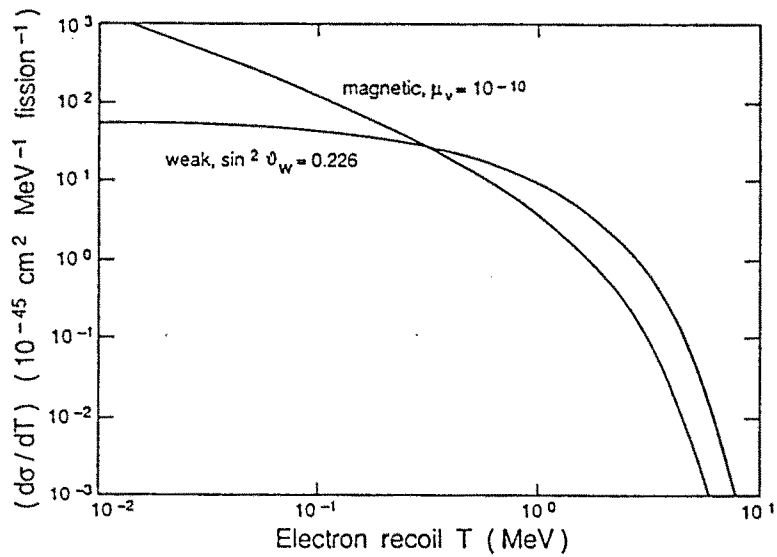


Fig. 14. Contribution of the neutrino magnetic moment to the $\bar{\nu}_e e \rightarrow \bar{\nu}_e e$ scattering, averaged over the reactor $\bar{\nu}_e$ spectrum. The purely weak cross section is also shown. (From Vogel and Engel¹¹)

